



# Quantum information scrambling and chemical reactions

Chenghao Zhang<sup>a,1</sup>, Sohang Kundu<sup>b,1</sup>, Nancy Makri<sup>a,b,2</sup>, Martin Gruebele<sup>a,b,c,d,2</sup>, and Peter G. Wolynes<sup>e,f,g,2</sup>

Contributed by Peter G. Wolynes; received December 8, 2023; accepted February 22, 2024; reviewed by Srihari Keshavamurthy and David M. Leitner

The ultimate regularity of quantum mechanics creates a tension with the assumption of classical chaos used in many of our pictures of chemical reaction dynamics. Out-of-time-order correlators (OTOCs) provide a quantum analog to the Lyapunov exponents that characterize classical chaotic motion. Maldacena, Shenker, and Stanford have suggested a fundamental quantum bound for the rate of information scrambling, which resembles a limit suggested by Herzfeld for chemical reaction rates. Here, we use OTOCs to study model reactions based on a double-well reaction coordinate coupled to anharmonic oscillators or to a continuum oscillator bath. Upon cooling, as one enters the tunneling regime where the reaction rate does not strongly depend on temperature, the quantum Lyapunov exponent can approach the scrambling bound and the effective reaction rate obtained from a population correlation function can approach the Herzfeld limit on reaction rates: Tunneling increases scrambling by expanding the state space available to the system. The coupling of a dissipative continuum bath to the reaction coordinate reduces the scrambling rate obtained from the early-time OTOC, thus making the scrambling bound harder to reach, in the same way that friction is known to lower the temperature at which thermally activated barrier crossing goes over to the low-temperature activationless tunneling regime. Thus, chemical reactions entering the tunneling regime can be information scramblers as powerful as the black holes to which the quantum Lyapunov exponent bound has usually been applied.

path integral | quantum chaos | wavefunction | activation energy | black holes

Most discussions of chemical kinetics assume that quantum information about the reactants is scrambled in the course of the reaction event. There are well-known exceptions to this commonplace idea. In many gas-phase reactions involving small molecules, the reaction cross-section depends on the specific initial vibrational excitation, not just the total energy (1-4). Conversely, products are formed in specific excited states in chemical lasers (5) and in bioluminescence (6). Whether quantum mechanical (QM) phase information is crucial to the efficiency of photosynthesis remains a topic engendering debate (7–12). These phenomena all require understanding and quantifying incomplete scrambling of quantum information by chemical reaction events.

The question of the extent of quantum information scrambling in chemical reactions can be addressed using the out-of-time-order correlator (OTOC). OTOCs provide a key mathematical tool to quantify how quickly information is scrambled in quantum systems. They have been employed in studies of black holes (13), many-body localized systems (14), diatomic molecules (15), and most recently in studying quantum information scrambling in vibrating molecules (16) as well as in double-well-oscillator systems using approximate quantum dynamics (17). The OTOC embodies the quantum analog of the Lyapunov exponent employed to quantify the instability of chaotic classical dynamical systems (18). The OTOC arises formally when we try to quantify the analogous instability to perturbation in quantum mechanics by computing the expectation value of the square of a commutator [A(0), B(t)]. This commutator in the classical limit would become a Poisson bracket that measures how sensitively an observable B at time t depends on making an initial change to A at time 0. The resulting square involves products of A(0) and B(t) in an order different from the usual one encountered in studying nonlinear responses of quantum averages to perturbations where, once the operator product is written out explicitly, the times follow each other sequentially. The OTOC gives an idea of how information concerning A at an initial time determines the value of B at a later time in a quantum system. In a classically chaotic system, the corresponding object, for a time, will grow exponentially. This growth in quantum mechanics must stop once the wave packet starts to sample the whole state space thoroughly at the resolution of the quantized levels. The sum of the exponential growth rates (for a complete set of observables) provides the so-called Kolmogorov-Sinai entropy (19, 20) or effective information spreading rate of an initial packet of trajectories.

# **Significance**

The "butterfly effect" causes the beating of an insect wing to change history, but how does this phenomenon manifest itself at the quantum level of chemical reactions, where atoms and electrons move about? We show, using fully quantum-mechanical wavefunction and path integral calculations of a simple chemical reaction, that scrambling of information in certain types of reactions can be nearly as fast as nature's ultimate information scrambler, a black hole. At the same time, the rate can approach the "prefactor" of transition state theory for such reactions, assisted by tunneling and by molecular vibrations.

Author affiliations: <sup>a</sup>Department of Physics, University of Illinois Urbana-Champaign, IL 61801; <sup>b</sup>Department of Chemistry, University of Illinois Urbana-Champaign, IL 61801; <sup>C</sup>Center for Biophysics and Quantitative Biology, University of Illinois at Urbana-Champaign, IL 61801; <sup>d</sup>Carle-Illinois College of Medicine, University of Illinois at Urbana-Champaign, IL 61801; <sup>e</sup>Department of Chemistry, Rice University, Houston, TX 77251; Department Physics, Rice University, Houston, TX 77251; and gCenter for Theoretical Biological Physics, Rice University, Houston, TX 77251

Author contributions: C.Z., S.K., N.M., M.G., and P.G.W. designed research; performed research; analyzed data; and wrote the paper.

Reviewers: S.K., Indian Institute of Technology; and D.M.L., University of Nevada.

The authors declare no competing interest.

Copyright © 2024 the Author(s). Published by PNAS. This article is distributed under Creative Commons Attribution-NonCommercial-NoDerivatives License 4.0 (CC BY-NC-ND).

<sup>1</sup>C.Z. and S.K. contributed equally to this work.

<sup>2</sup>To whom correspondence may be addressed. Email: nmakri@illinois.edu, mgruebel@illinois.edu, or pwolynes@

This article contains supporting information online at https://www.pnas.org/lookup/suppl/doi:10.1073/pnas. 2321668121/-/DCSupplemental.

Published April 1, 2024.

Quantum mechanics suggests a thermodynamic bound on the rate of information scrambling (21–27). In particular, Maldacena et al. (21) argue that the scrambling rate for a system at temperature T cannot exceed  $\lambda_{\rm M} = 4\pi^2 k_{\rm B} T/h$ , and we use their definition here. As mentioned in our previous paper (16), the exact analog to the classical Lyapunov exponent is  $^1/_2\partial \ln(s)/\partial t$ , but here as well as in ref. 16, we plot  $\partial \ln(s)/\partial t \le \lambda_{\rm M}$ , as is customary in the quantum scrambling community. The suggested bound has attracted much interest in the theory of black holes whose size endows them with a temperature (13) and in string theory (28). It also features in the properties of "strange metals" (29). The bound is saturated for black holes, which have been called out as being the most effective possible information scramblers (30).

In this paper, we will explore quantum information scrambling and reaction rates in simple models of a chemical reaction, where a molecule passes over a potential barrier to form a product. To approximate irreversible behavior, there must be additional vibrational degrees of freedom into which the information can scramble. In the model studied here, the calculations show that the rate of scrambling decreases slightly as the temperature of the system is lowered, while the reaction eventually switches from thermally activated dynamics to a tunneling-dominated regime. Upon still further cooling, the OTOC becomes oscillatory in small systems. The onset of this quiescent regime, taking over from thermal activation, occurs when deep tunneling becomes the main mechanism for the reaction. We study both of these regimes using basis set wavefunction calculations and real-time path integral methods.

We will see that since the proposed bound for the quantum scrambling rate decreases with decreasing temperature, it turns out this bound can be nearly saturated by the scrambling rate in the chemical reaction problem when the activation barrier and temperatures are low enough, just as the tunneling regime is entered upon cooling. In simple systems, tunneling dominates when the unstable mode frequency at the barrier top exceeds  $k_{\rm B}T/h$  (31, 32). In such a case, the chemical reaction rate can approach both the scrambling rate and Herzfeld's limiting rate  $k_{\rm H} = k_{\rm B}T/h$  (33) if the barrier is sufficiently low.

Herzfeld's limiting rate  $k_{\rm B}T/h$  is, of course, quite familiar in chemical physics, where it appears as the prefactor in transition state theory (34). Transition state theory suggests that this limiting reaction rate represents the maximum rate that can be found in the presence of a very small barrier, when the barrier top is thermally populated. Incidentally,  $k_{\rm B}T/h$  had been identified years before the development of modern quantum mechanics, let alone transition state theory, by Herzfeld as the maximum rate of gaseous atomic recombination (33).

Both the bound for the scrambling rate and Herzfeld's limit for the reaction rate ultimately can be traced back to the Heisenberg uncertainty principle, which not only determines the size of the smallest meaningful cell in phase space but also the interplay of time and energy. When one approaches these quantum limits from the classical regime, new phenomena inevitably occur. For example, in electron transport in disordered materials, one reaches the Ioffe–Regel limit when the mean free path of the electron comes close to the electron thermal De Broglie wavelength (35, 36). In this case, the electrons in disordered conductors begin to become localized. As another example, at sufficiently low temperature, a dilute gas of bosons stops being described at all by the classical kinetic theory of randomly colliding individual particles and becomes degenerate, undergoing Bose-Einstein condensation. Bose condensation or Fermi degeneracy probably provides the new physics in the atomic recombination example put forward originally by Herzfeld. This phenomenon may have been observed recently (37). Once in the strongly quantum regime, all these

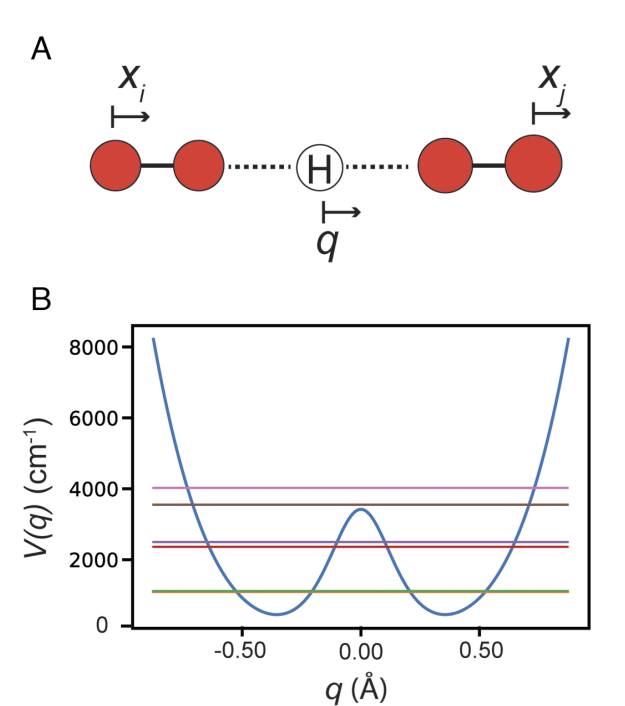


**Fig. 1.** Reaction model and reaction coordinate. (A) A sketch of the motif of the proton transfer reaction model, illustrating the reaction coordinate q and vibrational modes  $x_i$  and  $x_j$ . (B) The 1-D double-well potential used in this study  $V(q) = a_b {\rm sech}^2(q/q_b) + a_w(q/q_w)^4$  along the reaction coordinate q and its low-lying eigenstate energies. ( $a_b = 3,420~{\rm cm}^{-1}, q_b = 0.175~{\rm Å}, a_w = 2,140~{\rm cm}^{-1}, q_w = 0.625~{\rm Å};$  eigen-energies are 1,100 and 1,116 cm $^{-1}$  for the lowest tunneling doublet, 2,363 and 2,501 cm $^{-1}$  for the next one, and 3,555 and 4,028 cm $^{-1}$  for the states above the barrier top. For the reaction system, the 1-D double-well potential is coupled to  $N_b = 5~{\rm bath}$  modes with mean frequency  $<\omega>\approx 202~{\rm cm}^{-1}$ ). The bath modes are all coupled to one another by anharmonic couplings typical of molecular bending or stretching resonances in organic systems. See *SI Appendix, Supplementary Material section A* and Table S1 for details of the parameters used in Figs. 2–6.

systems become more quiescent than the purely classical arguments would have suggested and the quantum delocalized states are less sensitive to local perturbations than the classical trajectories would be.

## **Results and Discussion**

# Illustrative Results of Lyapunov Exponents and Reaction Rates.

In this section, for two illustrative examples, we compute the quantum scrambling rate given by the Lyapunov exponents  $\lambda_i$  obtained from the OTOCs and the effective reaction rates k(T) obtained from the Kubo-transformed population, or side–side (38, 39), correlation function  $C_{\rm PP}$  (which measures the time-dependent correlation of the reactant well population, see Methods). (31, 40–42) In our model, a molecule can pass over (or through) a potential barrier along a reaction coordinate "q", such as an isomerization or proton transfer coordinate (Fig. 1A), to form a product (39, 40). The reaction coordinate is coupled to five low-frequency vibrational (e.g., torsional) "bath" degrees of freedom.

We shall see that tunneling expands the accessible state space of the system, and that relatively low-frequency vibrations promote rapid growth of the OTOC early on, thus increasing scrambling even further than tunneling does on its own. As our first example, the double-well potential along the reaction coordinate is shown in Fig. 1*B*. We bilinearly couple it to  $N_{\text{bath}} = 5$  vibrational bath degrees of freedom (see *Methods* and *SI Appendix* for parameters) with average bath mode frequency  $<\omega>\approx 202 \text{ cm}^{-1}$ , typical

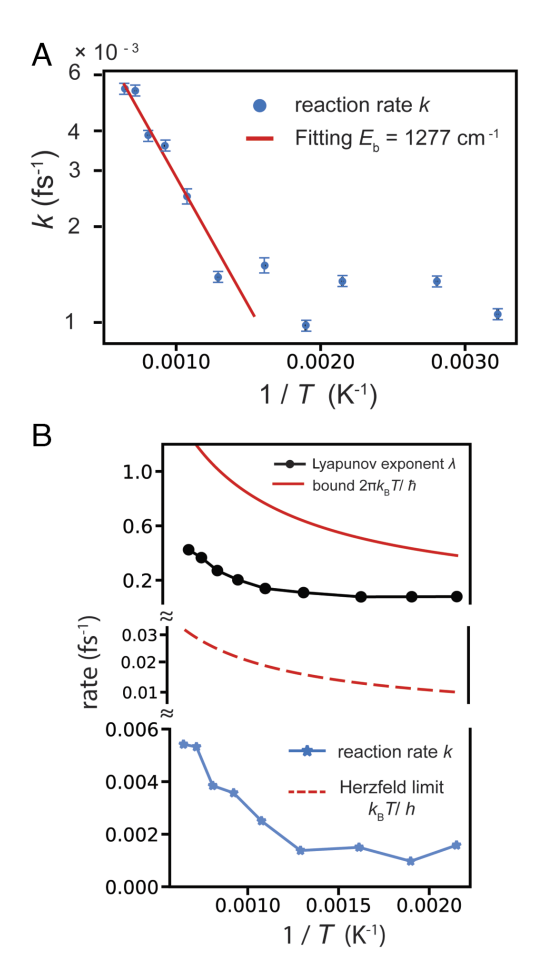


**Fig. 2.** Reaction rates and Lyapunov exponents for a proton transfer reaction model with a modest barrier. (*A*) The computed reaction rate k(T) (blue data points) at several different temperatures between 310 K and 1,550 K, (vertical axis on a logarithmic scale). The reaction rate in the thermal activation regime obeys the Arrhenius law (red line) with an effective barrier height  $E^{\sharp}=1,277$  cm<sup>-1</sup>; (*B*) The largest quantum Lyapunov exponent  $\lambda$  (black,  $\lambda_{\text{bath},1}$  as defined in the text) and the reaction rate k(T) (blue) as a function of reciprocal temperature approaches, but remains below, the bound  $\lambda_{\text{M}}=4\pi^2k_{\text{B}}T/h$  (red curve). The rate remains well below the Herzfeld limit  $k_{\text{H}}=k_{\text{B}}T/h$  (dashed red curve).

of low-frequency modes such as torsions, which we couple anharmonically to each other with coupling strength  $V_m = V_3 a^{m-3}$ , where m is the quantum number difference between states,  $V_3 = 0.1 < \omega >$  and a = 0.2 (see ref. 43 and *Methods* for details, *SI Appendix*, Table S1 for full parameter list).

We computed the Kubo-transformed side—side correlation function  $C_{\rm PP}(t)$  (*Methods*), from which we extract the effective reaction rate k(T) for this low-dimensional model at different temperatures T. Fig. 2A shows the reaction rate k(T) on a logarithmic vertical axis vs.  $\beta = 1/k_{\rm B}T$ . At high temperature, the rate obeys the Arrhenius law  $k(T) = A \exp(-E^{\rm T}/k_{\rm B}T)$  with a fitted effective barrier height  $E^{\rm T} = 1,277~{\rm cm}^{-1}$  which is less than the total classical barrier height. The small effective activation energy corresponds to the reaction occurring through the first excited doublet of states seen in Fig. 1B. As the temperature is lowered, the rate begins to level off.

To analyze the quantum scrambling in this multidimensional model, we computed the thermally averaged quantum OTOC matrix of the momenta and coordinates  $L_{ij}(t) = \left( \left[ x_i(t), p_j(0) \right]^2 \right)$ , from which we extracted the eigenvalues  $s_i(t)$  and quantum Lyapunov exponents  $\lambda_i = \partial \ln(s_i)/\partial t$  (see the *Methods* section and ref. 16 for details). In Fig. 2B, we show the reaction rate k(T) and

also the largest of the Lyapunov exponents  $\lambda_{\text{bath},1}(T)$  that reflects the rate of scrambling in the bath modes (see *SI Appendix, Supplementary Material section B* for details; in this case, the largest Lyapunov exponent  $\lambda$  corresponds to the bath coordinates). We additionally display the quantum bound on information scrambling proposed by Maldacena, Shenker, and Stanford,  $\lambda_{\text{M}}(T)$ . We see that the scrambling rate  $\lambda$  is significantly larger than the reaction rate k, and that the scrambling rate  $\lambda(T)$  approaches  $\lambda_{\text{M}}(T)$  at low temperature, while the reaction rate remains below the Herzfeld limit  $k_{\text{B}}T/h$ . As will be discussed further in *SI Appendix, Supplementary Material section C*,  $\lambda$  reflects all the scrambling mechanisms, such as vibrational anharmonicity, while k(T) primarily depends on the barrier-crossing process via activated or tunneling dynamics.

As a more extreme example, we computed results for a similar 6-D model with a narrower barrier (0.08 Å) that promotes tunneling, along with a lower-frequency anharmonic bath that reduces dissipation (Fig. 3A). The reaction coordinate again is coupled bilinearly to  $N_{\rm bath} = 5$  bath modes with an average frequency  $<\omega>\approx 40$  cm<sup>-1</sup> typical of low-frequency modes in

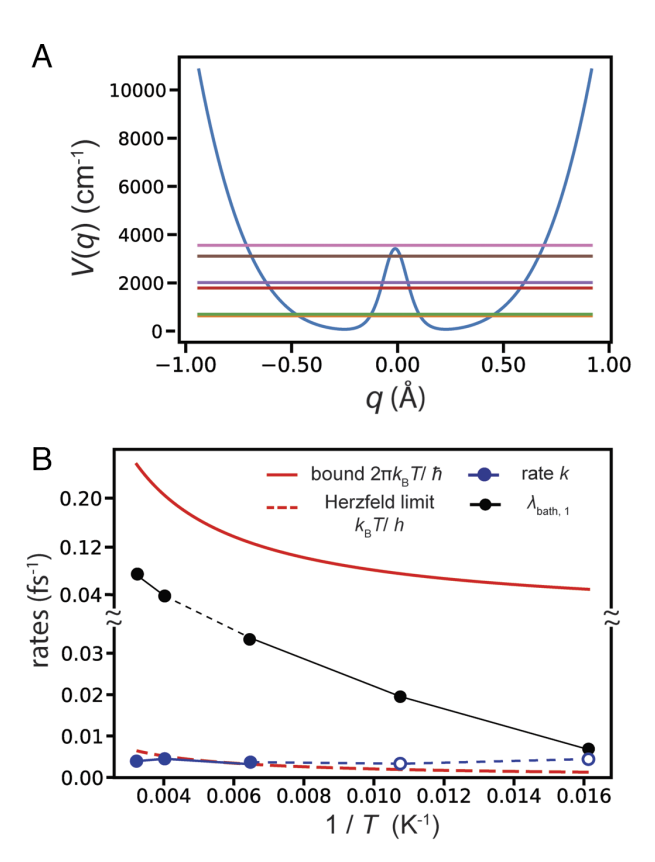


Fig. 3. Lyapunov exponents and reaction rates for an isomerization or proton transfer reaction with a low, narrow barrier and low-frequency bath. (A) The double-well potential along the reaction coordinate q is coupled to  $N_b = 5$ bath modes with mean frequency  $<\omega>$  = 40 cm<sup>-1</sup>, which corresponds to lowfrequency vibrational modes in proteins. The bath modes are coupled among themselves by anharmonic couplings. See SI Appendix, Supplementary Material section A and Table S2, for details of the parameters used in Figs. 3 and 4. (A) The double-well potential is  $V(q)=a_{\rm b}{\rm sech}^2(q/q_{\rm b})+a_{\rm w}(q/q_{\rm w})^4$  along the reaction coordinate q and its low-lying eigenstate energies are 639 and 702 cm<sup>-1</sup> for the lowest tunneling doublet, 1,795 and 2,016 cm<sup>-1</sup> for the next one, and 3,112 and 3,565 cm<sup>-1</sup> for the states at the barrier top ( $a_b$  = 3,420 cm<sup>-1</sup>,  $q_b$ = 0.08 Å,  $a_{\rm w}$  = 2,140 cm<sup>-1</sup>,  $q_{\rm w}$  = 0.625 Å (*B*) Effective reaction rate *k*(*T*) from the side-side correlation function (blue points) and Lyapunov exponent  $\lambda_{\text{hath 1}}(T)$ (black points) at different temperatures from 62 K to 310 K. For reference, we also plot the quantum scrambling bound  $4\pi^2k_BT/h$  (red curve) and Herzfeld limiting rate  $k_{\rm B}T/h$  (dotted red curve). Below about 155 K, the correlation function  $C_{PP}$  becomes oscillatory, so the rate becomes ill-defined (open circles).

macromolecules such as proteins. The bath modes are still coupled to each other via Fermi resonant couplings. Below 310 K, this system is in the deep tunneling regime where >95% of the equilibrium population can be found in the lowest tunneling doublet (see *SI Appendix*, Table S2 for parameters).

In Fig. 3B, we show the effective reaction rate k(T) obtained from the numerically computed side-side correlation function  $C_{\rm pp}(t)$ . Strictly speaking, the correlation function (40–42) does not unambiguously reach a plateau in this case (SI Appendix, Fig. S1), owing to the small number of degrees of freedom. The effective rate  $k(T) \approx 0.004 \text{ fs}^{-1}$  obtained in this way nevertheless is approximately constant in the tunneling regime. The Eyring expression for the rate of passage over the barrier classically at T = 310 K, gives  $k \approx k_B T/h \exp[-E^{\ddagger}/k_B T] = 1.8 \times 10^{-3} \text{ ns}^{-1}$ , which is much smaller than the calculated rate. In Fig. 3B, we also show the largest Lyapunov exponent characteristic of the bath modes (see SI Appendix, Supplementary Material section B for discussion of the full Lyapunov spectrum), along with the quantum bound on scrambling. The reaction rate k(T) now approaches the Herzfeld limit. The reaction rate also approaches the largest bath Lyapunov exponent  $\lambda_{\text{bath},1}(T)$ , which therefore lies below the bound. At temperatures below 62 K, the population correlation function  $C_{PP}$ becomes oscillatory and thus an effective reaction rate can no longer strictly be defined for this double well coupled to 5 bath modes.

Effect of Temperature and Anharmonicity on the Lyapunov **Spectrum.** For the same model as in Figs. 3 and 4A shows how the anharmonic couplings between bath modes contribute to quantum scrambling. We find that the eigenvector  $\vec{v}_0(t)$  of the largest OTOC eigenvalue aligns well with the reaction coordinate q, therefore, we denote this eigenvalue, which measures scrambling along the reaction coordinate primarily, as  $s_r(t)$ . The remaining eigenvectors align well with the individual vibrational bath modes so their eigenvalues are designated as  $s_{bath,i}(t)$ , with i = 1 corresponding to the largest eigenvalue. If the anharmonic coupling among bath modes is switched off, s<sub>bath,1</sub> initially remains small, growing later as a result of coupling to the tunneling system and indirect coupling to the other bath modes (44). As the anharmonic couplings are increased, we see an earlier onset of growth and a larger eigenvalue indicative of there being a larger accessible state space. Recent work identified signatures of chaotic dynamics in harmonic bath modes that couple strongly to a system by means of indirect coupling through the reaction coordinate (44). This scrambling of the bath modes makes it possible to define an effective reaction rate k(T) by fitting the side-side correlation function (SI Appendix, Fig. S1A), even though the flux-side correlation function does not have a plateau (SI Appendix, Fig. S1B). Such scrambling requires a sufficiently high temperature; in our model, this happens at about 155 K. SI Appendix, Fig. S2 illustrates all the Lyapunov eigenvalues  $s_{bath,I}$  at temperatures of T = 31 K and T = 465 K. At the lower temperature, only s<sub>bath,1</sub> shows a noticeable growth. In contrast, at the higher temperature, all OTOC eigenvalues  $s_{bath,i}$  show growth from which a Lyapunov exponent can be fitted. SI Appendix, Fig. S3 shows how the population correlation function  $C_{PP}$  smooths out and decays to 0.5 as 155 K is approached in the model of Fig. 3 and SI Appendix, Fig. S4 illustrates how two initial conditions of the simulation lead to thermalization of the bath mode energies.

For zero anharmonic couplings, Fig. 4*B* displays all the eigenvalues  $s_i(t)$  of the quantum thermal OTOC  $L_{ij}(t)$ . After the "ballistic time"  $\tau_{1d}$ , which is the time for the wave packet to sample a well in the 1-D reaction coordinate (see blue trace in Fig. 4*B*), all OTOC eigenvalues grow together by an order of magnitude before

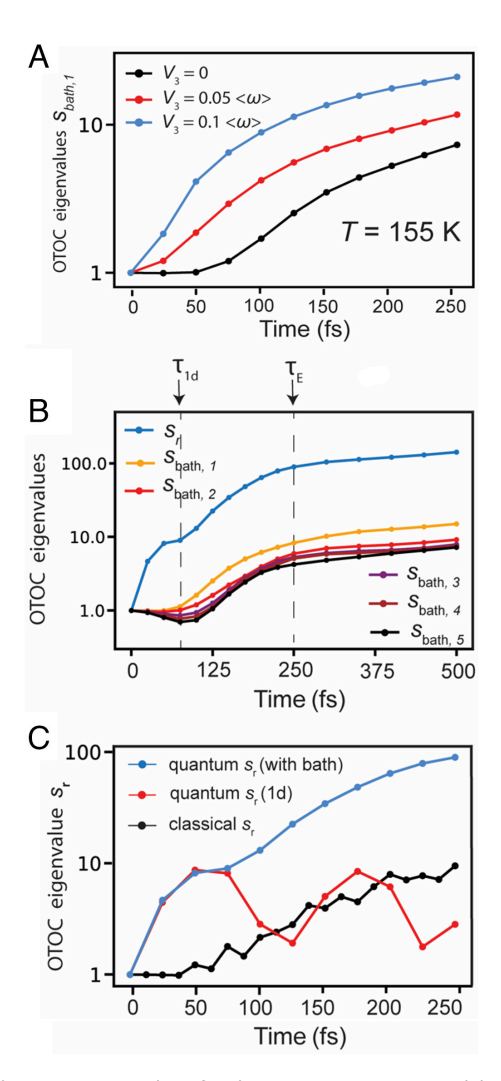


**Fig. 4.** The OTOC eigenvalues for the reaction in Fig. 3 (Model 2). (*A*) The effect of anharmonic couplings on the bath OTOC eigenvalues  $s_{\rm bath,i}$  (i = 1,...,5) (mostly along bath modes) at T = 155 K. We see the quantum scrambling rate increases upon introducing the anharmonic couplings among the bath modes (*B*) The eigenvalues  $s_r$  (eigenvector points mostly along the reaction coordinate) and  $s_{\rm bath,i}$  (eigenvector points along a linear combination of bath modes) at T = 310 K. The OTOC eigenvalues  $s_r$  grow between the "ballistic time"  $\tau_{10}$  and the "Ehrenfest time"  $\tau_{\rm E}$ , and we fit them to an exponential model in that time range to extract the Lyapunov exponents. (C) The slope of the eigenvalue  $s_r$  (which gives the Lyapunov exponent) from the quantum OTOC in panel (*B*) in the presence of even a small  $N_{\rm bath}$  = 5 bath (blue) matches the slope of the classical 1-D result (black), in contrast to the 1-D quantum eigenvalue (red), which oscillates.

leveling off. At the later "Ehrenfest time"  $\tau_{\rm E}$ , defined here as the time when the quantum system reaches its maximum scrambling consistent within the size of the accessible state space, the OTOC eigenvalues start to level off.

To analyze how the bath modes affect scrambling along the reaction coordinate q, we calculated the classical analog of  $s_r$  for 1-D dynamics along the reaction coordinate by using the thermal average  $L^c(t) = \left\langle \left| \partial q(t) / \partial q(0) \right|^2 \right\rangle$  (ref. 16 and *Methods*). This classical analog is calculated by averaging OTOCs over 2,000 classical trajectories with initial thermal distribution at temperature T (see *Methods* and *SI Appendix*, *Supplementary Material section B*). In Fig. 4C, the 1-D classical (black) and 6-D quantum  $s_r$  (blue) have the same slope between  $\tau_{1d}$  and  $\tau_{E}$ , whereas the quantum OTOC evaluated using only 1-D dynamics along the reaction coordinate yields oscillatory behavior (red). Through coupling to the small anharmonic bath, the quantum OTOC is allowed to

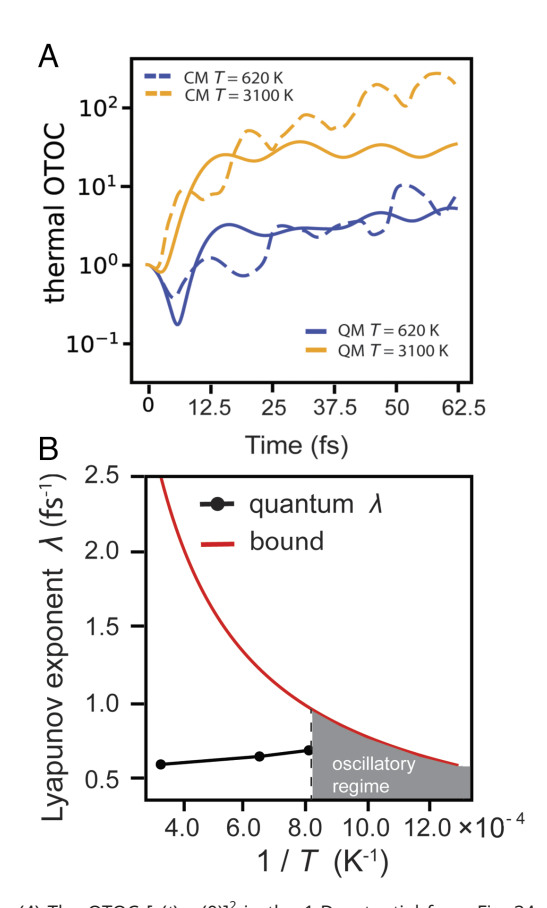


**Fig. 5.** (A) The OTOC [x(t), p(0)]<sup>2</sup> in the 1-D potential from Fig. 3A; (A) The quantum OTOC (solid curves) and the classical OTOC (dashed curves) at temperatures T = 620 K (blue) and 3,100 K (orange). (B) Computed thermal Lyapunov exponent  $\lambda(T)$  as a function of 1/T for the 1D double-well potentials (black dots). For reference, we also plot the bound  $\lambda_{\rm M} = 4\pi^2k_{\rm B}T/h$  in red. See *SI Appendix, Supplementary Material section B* for the fitting procedure.

grow such that the fitted quantum Lyapunov exponents are nearly the same as those of its classical counterpart.

For the few-mode system that we studied in Figs. 3 and 4, we see that coupling of the reaction coordinate to the five bath modes allows the quantum OTOC to grow with a fitted Lyapunov exponent  $\lambda$  having a similar magnitude as the classical Lyapunov exponent  $\lambda_C$ , thereby restoring the quantum–classical correspondence at all but the lowest temperatures, where tunneling allows near-saturation of the bound (Fig. 3). This, however, is not the only effect that coupling to bath modes can have on the OTOC. We already surmised that the original rapid increase of the OTOC is at least in part due to vibrational anharmonicity in the reactive coordinate (Figs. 2 and 4C). We will examine this idea further by considering as a limiting case the bare 1-D dynamics along the reaction coordinate from Fig. 3. In Fig. 5A, we compare the 1-D QM and classical mechanical OTOCs for the bare 1-D potential from Fig. 3A. At a temperature T = 3,100 K and time t < 12.5 fs, before the quantum OTOC levels off, the quantum and classical OTOCs grow at a similar rate, due mainly to 1-D anharmonicity in the potential well because tunneling does not play a role in the classical limit and at very early times. In Fig. 5B, the Lyapunov exponent  $\lambda = \partial (\ln(s))/\partial t$  calculated from the 1-D OTOC nearly saturates the quantum scrambling bound as the temperature is lowered (black points vs. red curve), until the OTOC becomes oscillatory at low temperature and  $\lambda$  can no longer be clearly defined (gray area in Fig. 5B). This bound on the quantum scrambling rate in 1-D systems can be traced back to the Heisenberg

uncertainty principle because it is not possible to scatter fully a wave whose wavelength at low temperature exceeds the characteristic length scale of the potential (23, 24). In *SI Appendix, Supplementary Material section C* and Fig. S5, we illustrate this point by studying how motions in different regions of the potential surface along the reaction coordinate contribute to quantum scrambling in the 1-D case.

The Damping Regime Due to a Continuum Bath. In a different regime explored below, decoherence from baths with a wide distribution of higher frequencies quenches OTOC growth, thus damping the dynamics and restoring low scrambling rates, leading ultimately to a stable state. This case is relevant when strong coherences can be set up, as in the case of excitation energy transfer in molecular dimers (45); in such a case, the motion between the wells resembles spin relaxation in NMR spectroscopy. To illustrate this regime, we studied a system having the quartic-Eckart tunneling coordinate from Fig. 1*B* coupled to a continuum bath of harmonic degrees of freedom with sufficient spectral density at high frequencies relative to the tunneling splitting, which is now set to 5 cm<sup>-1</sup>, to significantly damp the reaction coordinate (Methods). Continuous baths arise from the collective motions of condensed phase and biological environments, and their main effect on the reaction coordinate is to eventually lead the reactant and product wells to equilibrium. In spite of their simple form, harmonic bath models can often realistically capture the effects of large environments (liquids and biological molecules) whose interactions at the microscopic level may be complex and strongly anharmonic (42, 46). Such behavior is a consequence of the central limit theorem, which gives rise to Gaussian response. Further, even in the absence of direct coupling between them, the harmonic bath modes are able to exchange energy through indirect coupling with the reaction coordinate (44).

Fig. 6 shows the results for such a continuum bath, obtained by propagating the density matrix for the reaction coordinate using the quasi-adiabatic propagator path integral (QuAPI) algorithm (47, 48) (see *SI Appendix*, Table S3 for parameters).

In the absence of coupling to the bath, the OTOC for the reaction coordinate (black curve, calculated by a wavefunction approach as in Figs. 2–5) oscillates, much like the 1-D OTOC shown in Fig. 4C. The slow oscillations (ca. 0.8 ps period) arise from the tunneling doublet, while the superposed small-amplitude,

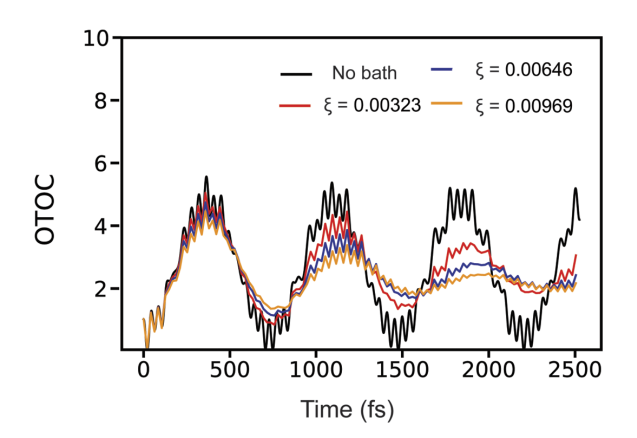


**Fig. 6.** Thermal OTOC at the temperature  $T=620~{\rm K}$  for a system-bath Hamiltonian with a continuum harmonic bath. The system potential is shown in Fig. 1*B.* The bath spectral density has the form  $J(\omega)=h\xi\omega\exp(-\omega I\omega_c)$ , with  $\omega_c=1,250~{\rm cm}^{-1}$  and  $\xi=0.00323$  to 0.00969. The thermal OTOC without the bath (black curve) oscillates mainly due to tunneling, and is damped when coupled with the bath (red, blue, and orange curve).

high-frequency oscillations result from motion within each of the two potential wells. When coupling to the harmonic bath is introduced (colored curves), the slow tunneling oscillations of the OTOC are gradually damped, while the high-frequency oscillations are only mildly affected. These effects are analogous to those that govern the time evolution of the probability for a system initially equilibrated within the reactant well. The oscillations are gradually washed away in amplitude because the bath induces dephasing (a "T2" effect) and because of energy loss from the system into the continuum bath (a " $T_1$ " effect). This classification of behaviors is familiar from Redfield calculations, such as those used for coherent reaction models of photosynthesis (49). Finally, we observe that the 0.8 ps time period of tunneling oscillations is slightly prolonged by the system-bath interactions. This is a typical signature of suppression of the system's tunneling splitting by high-frequency bath modes (50, 51).

Since the collective effect from an infinity of bath modes is finite, each of the modes is weakly coupled to the reaction coordinate. Recent work on a similar (nonadiabatic, rather than tunneling) model (44) showed that the quantum motion of bath oscillators is "regular" in the weak coupling limit, i.e., similar to that of classical systems that do not explore all of the phase space available to them and which do not display a high sensitivity to initial conditions. Thus, it is not surprising that such a bath does not cause a rapid growth of the OTOC above the maximum value attained through tunneling. In contrast, signatures of chaotic motion were observed (44) in modes that are strongly coupled to the system, indicative of exploration of a much larger state space and consistent with the existence of Lyapunov exponents. Such behavior is consistent with the rapid growth of the OTOC in Fig. 4A in the case of five bath modes with sizable coupling to the reaction coordinate, even when the anharmonic coupling among the bath modes is set to zero.

## **Conclusions**

Our calculations show that the reaction kinetics and quantum information scrambling are indeed intimately related: Some degree of scrambling is needed to establish even the basic phenomenology of kinetics. Information flow rates and barrier crossing rates deviate strongly from classical results when one enters a regime where the quantum tunneling through the barrier, assisted by additional low-frequency modes, starts to play a dominant role. As a function of temperature, deviations begin to occur when the bound proposed by Maldacena, Shenker, and Stanford for quantum scrambling is approached by the quantum Lyapunov exponent (Fig. 2). The bound on the Lyapunov exponent is approached more closely than the Herzfeld limit because the difficulty of barrier penetration by tunneling prevents the rate from approaching the Herzfeld limit in most cases. Nevertheless, reacting molecules having thin or low barriers can be maximally effective information scramblers whose quantum Lyapunov exponent nearly reaches the quantum scrambling bound (Fig. 2). For these, the reaction rate can approach the quantum Lyapunov exponent and the Herzfeld limit, provided the barrier is thin (Fig. 3). Chemical reactions can scramble information on a subpicosecond time scale, a rate which only the smallest of black holes are likely to reach.

Here, we have analyzed several simple models of reactions with isoenergetic reactants and products (e.g., isomerization, symmetric proton transfer) using the tools of quantum Lyapunov exponent analysis, accurate wavefunction calculations with a reaction coordinate coupled to a few resonantly coupled modes, and real-time path integral calculations for the case of a harmonic continuum bath. A full phase diagram of scrambling and reaction

rates for reactions with various degrees of exothermicity and couplings that encompasses all limiting cases, such as in Figs. 2, 3, and 6, remains to be constructed. We believe that the present tools already can be applied to look at many specific molecular systems, which may be accessed in the near future using spectroscopic methods (52).

#### Methods

**Model Hamiltonian.** The barrier-crossing process plays a central role in many areas of physical science, from black holes absorbing particles to chemical reactions absorbing a reactant. Here, we study a model quantum system that manifests barrier crossing in a simple way—the 1-D double-well potential  $V_{\rm DW}$ . The Hamiltonian can be expressed as  $H = p^2/2m + V_{\rm DW}(q)$ , where

$$V_{\rm DW}(q) = a_{\rm h} {\rm sech}^2(q/q_{\rm h}) + a_{\rm w}(q/q_{\rm w})^4.$$
 [1]

The Eckart potential in the first term introduces a barrier with tunable height  $a_b$  and width  $q_b$ , and the quartic potential in the second introduces an anharmonic well with tunable width.  $q_w$  that allows a wavepacket to dephase (Fig. 1A).

The OTOC of an isolated reaction coordinate can be studied using the 1-D quantum system described above. To study the dynamics of polyatomic molecules, additional modes can be included. The Hamiltonian for this system can be expressed as

$$H = p^2/2m + V_{DW} + V_{H} + V_{c} + V_{a},$$
 [2a]

where

$$V_{\rm H} = \sum_{i=1}^{n} p_i^2 / 2m + \frac{1}{2} m \omega_i^2 x_i^2,$$
 [2b]

$$V_{c} = \sum_{i=1}^{\infty} c_{i}qx_{i} + \frac{c_{i}^{2}q^{2}}{2m\omega_{i}^{2}},$$
 [2c]

and

$$V_{a} = \sum_{m} \prod_{i} V_{m} \left( b_{i}^{\dagger} \right)^{m_{i}^{\dagger}} b_{i}^{m_{i}^{-}}.$$
 [2d]

The term  $V_{\rm H}$  describes the harmonic oscillators.  $V_{\rm c}$  is the bilinear coupling potential.  $V_{\rm a}$  is the anharmonic vibrational coupling operator. We truncated the anharmonic coupling constants  $V_m$  at 4th order. The  $m = \{m_\alpha\}$  are integers that describe the order of the anharmonic vibrational couplings, e.g.,  $m_1^+ = 2$  and  $m_2^- = 1$  describe a cubic resonance between modes 1 and 2. Here, we choose to include only cubic coupling and quartic terms, by requiring the order of nonlinear coupling  $m = \sum_{\alpha} \left(m_1^\alpha + m_{\alpha}^-\right) = 3$  or 4. We use an average value of 10% of the frequency (e.g.,  $V_3 = 20$  cm $^{-1}$  for a 200 cm $^{-1}$  mode), typical of molecular anharmonicities of low-frequency vibrations.  $V_4$  is 0.2 of  $V_3$ , the average value for small organic molecules (53).

We denote the coupling strength for oscillator i as  $c_i$ , the coordinate along the Eckart-quartic potential as q and the harmonic oscillator coordinates as  $x_i$ . For the model calculation here, the linear coupling strengths  $c_i$  are set to  $c_i = c\sqrt{\langle\omega\rangle}\omega_i$ . The frequencies of the five-mode bath are set proportional to the frequencies of five normal modes of the bacteriochlorophyll molecule (54). The bath modes can also couple to each other through an anharmonic coupling  $V_{av}$  which facilitates scrambling between modes.

The continuous bath is described by a spectral density of the common Ohmic form, where the spectral density is defined in general as

$$J(\omega) = \frac{\pi}{2} \sum_{i} \frac{c_{i}^{2}}{m_{i} \omega_{i}} \delta\left(\omega - \omega_{i}\right).$$
 [3a]

And in our specific case, for an Ohmic bath, as

$$J(\omega) = h\xi \omega e^{-\omega/\omega_c},$$
 [3b]

where  $\xi$  is a parameter that quantifies the system-bath coupling strength.

Numerical Methods for OTOC Calculations. The regularized thermal OTOC is given by

$$L^{\{reg\}}(\beta, t) = -\text{Tr}[[q(t), \rho]e^{-\beta H/2}[q(t), \rho]e^{-\beta H/2}]/\text{Tr}[e^{-\beta H}].$$
 [4]

For a system with a few degrees of freedom, the OTOC can be obtained either by exact diagonalization of the Hamiltonian or by time-evolving an initial wave packet. The method for computing the OTOC by exact diagonalization is straightforward and can be found in ref. 55.

The thermal average of the OTOC can be approximated by taking the expectation values with respect to Haar random initial states using quantum typicality (22, 56-58)

$$\widehat{L}^{\{reg\}}(\beta,t) \approx -\frac{\sum_{r=1}^{R} \left\langle r | \left[ q(t), \rho \right] e^{-\beta H/2} \left[ q(t), \rho \right] e^{-\beta H/2} | r \right\rangle}{\sum_{r=1}^{R} \left\langle r | e^{-\beta H} | r \right\rangle}.$$
 [5]

We generate the Haar random states by drawing each element of the wave function |r| > from a Gaussian distribution. The error of this approximation can be reduced by averaging over several initial Haar states. In practice, we find that the average over R = 5 random overall states gives reliable results (59). We compute thermal OTOCs  $L^{\text{reg}}(t)$  by propagating the time-dependent Schrödinger equation forward and backward in time using the Chebyshev method (60). OTOCs computed using the exact diagonalization and wave function method agree with each other.

To analyze the scrambling in multidimensional models, we can compute the quantum OTOC matrix  $L_{ij}(t) = \left\langle \left[ x_i(t), p_j \right]^2 \right\rangle$  and classical OTOC matrix  $L_{ij}^c(t) = \left\langle \left| \partial x_i(t) / \partial x_j \right|^2 \right\rangle$ . By diagonalizing  $\widehat{L}(t)$  and  $\widehat{L}^c(t)$ , the time-dependent OTOC eigenvalues  $s_i(t)$  (or  $s_i^c(t)$ ) and corresponding OTOC eigenvectors  $\vec{v_i}(t)$  (or

 $\overline{v_i^c}(t)$ ) can be obtained. The eigenvalues  $s_i(t)$  characterize the scrambling along directions given by OTOC eigenvectors  $\vec{v_i}(t)$ . The Lyapunov exponent  $\lambda_i$ can be defined as  $\lambda_i(t) = \partial(\ln(s_i))/\partial t$  in the exponentially growing regime of  $s_i(t)$ . Note that here, we follow the convention in the literature to define the Lyapunov exponent as the exponential growth rate of the OTOC eigenvalue or the square of the classical sensitivity matrix. The Lyapunov exponent defined in this way is two times of the Lyapunov exponent as often defined in classical dynamical systems theory. This regime is short for small quantum systems, and we describe our fitting procedure in detail in SI Appendix, Supplementary Material section B.

- F. F. Crim, State- and bond-selected unimolecular reactions. Science 249, 1387 (1990).
- A. Sinha, M. C. Hsiao, F. F. Crim, Controlling bimolecular reactions: Mode and bond selected reaction of water with hydrogen atoms. J. Chem. Phys. 94, 4928 (1991).
- F. F. Crim, Chemical dynamics of vibrationally excited molecules: Controlling reactions in gases and on surfaces. Proc. Natl. Acad. Sci. U.S.A. 105, 12654 (2008).
- Y. S. Choi, C. B. Moore, State-specific unimolecular reaction dynamics of HFCO. I. Dissociation rates. J. Chem. Phys. **97**, 1010 (1992).
- J. V. V. Kasper, G. C. Pimentel, HCl chemical laser. Phys. Rev. Lett. 14, 352 (1965).
- E. H. White, E. Rapaport, T. A. Hopkins, H. H. Seliger, Chemi- and bioluminescence of firefly luciferin. J. Am. Chem. Soc. 91, 2178 (1969).
- J. Cao et al., Quantum biology revisited. Sci. Adv. 6, eaaz4888 (2020).
- G. D. Scholes, G. R. Fleming, A. Olaya-Castro, R. van Grondelle, Lessons from nature about solar light
- harvesting. Nat. Chem. 3, 10 (2011). A. Chenu, G. D. Scholes, Coherence in energy transfer and photosynthesis. Annu. Rev. Phys. Chem. 66, 69 (2015).
- M. B. Plenio, S. F. Huelga, Dephasing-assisted transport: Quantum networks and biomolecules.
- N. J. Phys. 10, 113019 (2008). M. Mohseni, P. Rebentrost, S. Lloyd, A. Aspuru-Guzik, Environment-assisted quantum walks in
- photosynthetic energy transfer. J. Chem. Phys. 129, 174106 (2008). S. Kundu, R. Dani, N. Makri, Tight inner ring architecture and quantum motion of nuclei enable
- efficient energy transfer in bacterial light harvesting. Sci. Adv. 8, eadd0023 (2022).
- S. H. Shenker, D. Stanford, Black holes and the butterfly effect. J. High Energ. Phys. 2014, 67 (2014). R.-Q. He, Z.-Y. Lu, Characterizing many-body localization by out-of-time-ordered correlation. Phys. Rev. B 95, 054201 (2017).
- H. Li, E. Halperin, R. R. W. Wang, J. L. Bohn, Out-of-time-order correlator for the van der waals potential. Phys. Rev. A 107, 032818 (2023).
- C. Zhang, P. G. Wolynes, M. Gruebele, Quantum information scrambling in molecules. Phys. Rev. A 105, 033322 (2022)
- V. G. Sadhasivam, L. Meuser, D. Reichman, S. C. Althorpe, Instantons and the quantum bound to chaos. Proc. Natl. Acad. Sci. U.S.A. 120, e2312378120 (2023).
- H. Gharibyan, M. Hanada, B. Swingle, M. Tezuka, Quantum lyapunov spectrum. J. High Energ. Phys. 2019, 82 (2019).
- I. Hamilton, P. Brumer, Intramolecular relaxation in N = 2 Hamiltonian systems: The role of the K entropy. J. Chem. Phys. 78, 2682 (1983).

Kubo Transformed Projection Operator Correlation Functions and Reaction Rates. To study the rates in reactive systems, we compute the Kubo-transformed side-

Rates. To study the rates in reactive systems, we compute the Kubo-transformed side-  
side correlation function 
$$C_{pp}(t) = Tr \left[ \frac{1}{\beta} \int_{0}^{\beta} e^{-(\beta-\beta')H} \widehat{P} e^{-\beta'H} \widehat{P} d\beta' \right] / Tr \left[ e^{-\beta H} \widehat{P} \right]$$

where  $\hat{P}$  is the projection operator onto the reactant well, not to be confused with the momentum operator p. In the system we studied here, the reactant population  $C_{PP}(t)$ exhibits effective rate behavior after an initial transient has died out.  $C_{PP}(t)$  decays according to the form  $C_{PP}(t) = C_{PP}(\infty) + [C_{PP}(t_{exp}) - C_{PP}(\infty)] \exp(-k(t - t_{exp}))$  (61), where  $t_{\rm exp}$  indicates the onset time of the exponential regime and k is the reaction rate. For the symmetric double well, the system equilibrates at  $C_{PP}(t \to \infty) = 0.5$ . For the fast reaction dynamics studied here, the lack of a clear separation of time scales between transient dynamics and exponential decay time can cause the correlation function to fail to display a plateau. In such cases, an effective rate k can still be obtained by fitting to the function given above.

#### Numerical Path Integral Methods for the Continuous Bath Hamiltonian.

We calculate the regularized thermal OTOC using an extension of the numerically exact QuAPI method (47, 48). The propagators and influence functional are evaluated in a discrete variable representation of the path integral expression (62). Since the OTOC comprises two sets of forward and backward time evolution operators separated by noncommuting operators, as well as two Boltzmann factors, the time contour of the path integral contains two branches, encompassing real- and imaginary-time components. The effect of the bath is included in the QuAPI-discretized influence functional, which is expressed in terms of coefficients evaluated from numerical integration of analytically obtained expressions that involve the spectral density (63, 64). The iterative QuAPI algorithm captures non-Markovian effects at finite temperatures.

Data, Materials, and Software Availability. All study data are included in the article and/or SI Appendix.

ACKNOWLEDGMENTS. C.Z. and M.G. were supported by the James R. Eiszner Chair in Chemistry. Computations were supported on Delta, funded by NSF grant ACI-1548562. C.Z. and M.G. are grateful to the School of Chemical Sciences Computing for support and access to the SCS HPC Cluster. P.G.W. was supported by the Center for Theoretical Biological Physics, NSF grant PHY- 2019745. Additionally, P.G.W. wishes to recognize the D. R. Bullard Welch Chair at Rice University, Grant C-0016. S.K. and N.M. were supported by the NSF under CHE-1955302.

- 20. P. Brumer, M. Shapiro, "Chaos and reaction dynamics" in Advances in Chemical Physics, I. Prigogine, S. A. Rice, Eds. (John Wiley & Sons Inc, Hoboken, NJ, 2007), pp. 365-439.
- J. Maldacena, S. H. Shenker, D. Stanford, A bound on chaos. J. High Energ. Phys. 2016, 106
- B. Kobrin et al., Many-body chaos in the Sachdev-Ye-Kitaev Model. Phys. Rev. Lett. 126, 030602
- S. Pappalardi, J. Kurchan, Low temperature quantum bounds on simple models. SciPost Phys. 13,
- J. Kurchan, Quantum bound to chaos and the semiclassical limit. J. Stat. Phys. 171, 965 (2018).
- S. Pappalardi, L. Foini, J. Kurchan, Quantum bounds and fluctuation-dissipation relations. SciPost Phys. 12, 130 (2022)
- C. Murthy, M. Srednicki, Bounds on chaos from the eigenstate thermalization hypothesis. Phys. Rev. Lett. 123, 230606 (2019).
- N. Tsuji, T. Shitara, M. Ueda, Bound on the exponential growth rate of out-of-time-ordered correlators. Phys. Rev. E 98, 012216 (2018).
- S. H. Shenker, D. Stanford, Stringy effects in scrambling. J. High Energ. Phys. 2015, 132 (2015).
- P. W. Phillips, N. E. Hussey, P. Abbamonte, Stranger than metals. Science 377, eabh4273 (2022).
- Y. Sekino, L. Susskind, Fast scramblers. J. High Energy Phys. 2008, 065 (2008).
- P. G. Wolynes, Quantum theory of activated events in condensed phases. Phys. Rev. Lett. 47, 968
- H. Grabert, U. Weiss, Crossover from thermal hopping to quantum tunneling. Phys. Rev. Lett. 53, 1787 (1984)
- K. F. Herzfeld, Zur Theorie der Reaktionsgeschwindigkeiten in Gasen. Ann. Phys. 364, 635 (1919).
- H. Eyring, The activated complex in chemical reactions. J. Chem. Phys. 3, 107 (1935)
- A. F. loffe, A. R. Regel, Non-crystalline amorphous, liquid electronic semiconductors. Prog. Semicond. 4, 237-291(1960).
- D. E. Logan, P. G. Wolynes, Dephasing and anderson localization in topologically disordered systems. Phys. Rev. B 36, 4135 (1987).
- Z. Zhang, S. Nagata, K.-X. Yao, C. Chin, Many-body chemical reactions in a quantum degenerate gas. Nat. Phys. 19, 1446-1470 (2023).
- W. H. Miller, S. D. Schwartz, J. W. Tromp, Quantum mechanical rate constants for bimolecular reactions. J. Chem. Phys. 79, 4889 (1983).
- R. Kubo, Statistical-mechanical theory of irreversible processes. I. General theory and simple applications to magnetic and conduction problems. J. Phys. Soc. Jpn. 12, 570 (1957).

- T. Yamamoto, Quantum statistical mechanical theory of the rate of exchange chemical reactions in the gas phase. J. Chem. Phys. 33, 281 (1960).
- W. H. Miller, Quantum mechanical transition state theory and a new semiclassical model for reaction rate constants. J. Chem. Phys. 61, 1823 (1974).
- D. Chandler, Statistical mechanics of isomerization dynamics in liquids and the transition state approximation. J. Chem. Phys. 68, 2959 (1978).
- D. Madsen, R. Pearman, M. Gruebele, Approximate factorization of molecular potential surfaces. I. Basic approach. J. Chem. Phys. 106, 5874 (1997).
- S. Kundu, N. Makri, Time evolution of bath properties in spin-boson dynamics. J. Phys. Chem. B 125, 8137 (2021).
- S. Kundu, N. Makri, Intramolecular vibrations in excitation energy transfer: Insights from real-time path integral calculations. Annu. Rev. Phys. Chem. 73, 349 (2022).
- N. Makri, The linear response approximation and its lowest order corrections: An influence functional approach. J. Phys. Chem. 103, 2823-2829 (1999).
- N. Makri, Improved feynman propagators on a grid and non-adiabatic corrections within the path integral framework. Chem. Phys. Lett. 193, 435 (1992).
- N. Makri, D. E. Makarov, Tensor propagator for iterative quantum time evolution of reduced density matrices. I. Theory. J. Chem. Phys. 102, 4600 (1995).
- J. N. Onuchic, P. G. Wolynes, Classical and quantum pictures of reaction dynamics in condensed matter: Resonances, dephasing, and all that. J. Phys. Chem. 92, 6495 (1988).
- 50. A. J. Leggett et al., Dynamics of the dissipative two-state system. Rev. Mod. Phys. 59, 1 (1987).
- R. Silbey, R. A. Harris, Variational calculation of the dynamics of a two level system interacting with a bath. J. Chem. Phys. 80, 2615 (1984).
- S. Asban, K. E. Dorfman, S. Mukamel, Interferometric spectroscopy with quantum light: Revealing out-of-time-ordering correlators. *J. Chem. Phys.* 154, 210901 (2021).

- R. Pearman, M. Gruebele, On the importance of higher order anharmonic molecular couplings. J. Chem. Phys. 108, 6561 (1998).
- C. Zhang, M. Gruebele, D. E. Logan, P. G. Wolynes, Surface crossing and energy flow in many-dimensional quantum systems. *Proc. Natl. Acad. Sci. U.S.A.* 120, e2221690120 (2023).
- K. Hashimoto, K. Murata, R. Yoshii, Out-of-time-order correlators in quantum mechanics. J. High Energ. Phys. 2017, 138 (2017).
- S. Goldstein, J. L. Lebowitz, R. Tumulka, N. Zanghì, Canonical typicality. *Phys. Rev. Lett.* 96, 050403 (2006).
- R. Steinigeweg, J. Gemmer, W. Brenig, Spin-current autocorrelations from single pure-state propagation. Phys. Rev. Lett. 112, 120601 (2014).
- 58. D.J. Luitz, Y. Bar Lev, Information propagation in isolated quantum systems. *Phys. Rev. B* **96**, 020406 (2017)
- J. Schnack, J. Richter, R. Steinigeweg, Accuracy of the finite-temperature lanczos method compared to simple typicality-based estimates. *Phys. Rev. Res.* 2, 013186 (2020).
- H. Tal-Ezer, R. Kosloff, An accurate and efficient scheme for propagating the time dependent schrödinger equation. J. Chem. Phys. 81, 3967 (1984).
- A. Bose, N. Makri, Non-equilibrium reactive flux: A unified framework for slow and fast reaction kinetics. J. Chem. Phys. 147, 152723 (2017).
- M. Topaler, N. Makri, System-specific discrete variable representations for path integral calculations with quasi-adiabatic propagators. Chem. Phys. Lett. 210, 448 (1993).
- N. Makri, Numerical path integral techniques for long time dynamics of quantum dissipative systems. J. Math. Phys. 36, 2430 (1995).
- J. Shao, N. Makri, Iterative path integral formulation of equilibrium correlation functions for quantum dissipative systems. J. Chem. Phys. 116, 507 (2002).